 MCB, vol.4, no.2, pp.75-85, 2007

# Modeling Ultrasonic Transient Scattering from Biological Tissues Including their Dispersive Properties Directly in the Time Domain

**G.V. Norton*** **and J.C. Novarini†**

**Abstract:** Ultrasonic imaging in medical applications involves propagation and scattering of acoustic waves within and by biological tissues that are intrinsically dispersive. Analytical approaches for modeling propagation and scattering in inhomogeneous media are difficult and often require extremely simplifying approximations in order to achieve a solution. To avoid such approximations, the direct numerical solution of the wave equation via the method of finite differences offers the most direct tool, which takes into account diffraction and refraction. It also allows for detailed modeling of the real anatomic structure and combination/layering of tissues. In all cases the correct inclusion of the dispersive properties of the tissues can make the difference in the interpretation of the results. However, the inclusion of dispersion directly in the time domain proved until recently to be an elusive problem. In order to model the transient signal a convolution operator that takes into account the dispersive characteristics of the medium is introduced to the linear wave equation. To test the ability of this operator to handle scattering from localized scatterers, in this work, two-dimensional numerical modeling of scattering from an infinite cylinder with physical properties associated with biological tissue is calculated. The numerical solutions are compared with the exact solution synthesized from the frequency domain for a variety of tissues having distinct dispersive properties. It is shown that in all cases, the use of the convolutional propagation operator leads to the correct solution for the scattered field.

* Naval Research Laboratory, Stennis Space Center, MS, USA.

† Planning Systems Inc., 21294 Johnson Rd, Long Beach, MS, USA.

**Keyword:** Acoustics, Finite-Difference, Time-Domain, Ultrasonic, Dispersion.

## 1 Introduction

Ultrasonic imaging in medical applications involves propagation through and scattering by biological tissues that are intrinsically dispersive, i.e., they present a frequency-dependent attenuation and associated frequency-dependent sound speed (dispersion). Analytical approaches to the problem of modeling the propagating and backscattered field in inhomogeneous media are difficult and invariably requires severe simplifying approximations in order to achieve a solution. Standard ultrasound imaging methods such as pulse echo techniques and tomography use either the scattered field or both the transmitted and scattered field to form a two-dimensional (2-D) image of the tissue under investigation. Clinical broadband pulse echo systems utilize the spectrum of the backscattered signal and relates it to the physical properties of the tissue, which is valuable for clinical diagnosis [Lizzi, Greenebaum, Feleppa, Elbaun, and Coleman (1983)]. Different tissues or different states of a tissue (benign, malignant) can then be discriminated by using broadband pulses in scattering and/or transmission. For example, breast tumours can be identified due to their high loss relative to the surrounding tissues [Manry and Broschat (1996)].

Numerical models applicable for ultrasound propagation and scattering in anatomic structures, are usually used to validate and calibrate image reconstruction algorithms. In general they are based on first order scattering approximations (weak scattering), either Born or Rytov approximations, which are also invoked in the algorithms for image reconstruction. As pointed out by Manry

and Broschat (1996), even in cases where scattering is weak (e.g., within a breast) the fat lobes near the surface of the breast strongly refracts the acoustic beam, thus invalidating the hypothesis of weak scattering. To avoid over simplification in modeling the acoustic field, direct solution of the wave equation via robust numerical methods (finite differences, finite elements, k-space methods, etc.) are desirable. They offer the most direct tool to produce numerical acoustic fields from which synthetic images of realistic anatomic structures can be generated, while fully accounting for diffraction, refraction, attenuation and dispersion.

When modeling transient propagation, the time-domain is the natural and more efficient domain to work in. Analytical and numerical approaches for modeling broadband pulses are usually the result of inverse Fourier transforming a collection of discrete frequency-domain solutions. In the case of inhomogeneous media, where propagation occurs in irregular shaped layered media with a collection of embedded scatters analytical approaches are limited by the severe approximations invoked in order to produce a solution. Most earlier efforts in direct time-domain numerical modeling through complex anatomical structures have either ignored dispersion and attenuation [Tabei, Mast, and Waag (2002);Tabei, Mast, and Waag (2003)] or assumed a frequency independent attenuation [Manry and Broschat (1996)]. One of the main uses of numerical modeling in medical ultrasound is to produce simulated acoustic fields upon which back propagation algorithms, tomographic reconstruction or imaging processes are then benchmarked. In all cases it is important to properly account for both attenuation and dispersion. Ignoring them leads to erroneous scattering amplitudes at interfaces, and incorrect overall losses and phase shifts in the propagating field. Exact inclusion of frequency dependent attenuation and its casual companion, dispersion into the linear wave equation (while remaining in the time-domain) can provide higher accurate numerical fields for benchmarking inverse reconstruction methods. However, until recently such inclusion remained elusive.

Recently, large scale simulation of ultrasonic pulse propagation through realistic anatomic cross sections have been performed [Mast, Hinkelman, Orr, Sparrow, and Waag (1997)] using a full-wave k-space method based on coupled first-order differential equations for linear acoustic propagation [Mast, Hinkelman, Orr, Sparrow, and Waag (1998)]. The model included attenuation and dispersion and presents low numerical intrinsic dispersion. The k-space method has been shown to be more efficient than a 2-4 finite-difference-time-domain (FDTD) solution for homogeneous soft tissues. However, it should be noted that the k-space model is not exact for inhomogeneous media. The spatial differential equations are solved globally by fast Fourier transforms (FFT), and temporal iteration is performed using a k-t space temporal propagator. The propagator is exact only for homogenous media. When scatterers of high impedance contrasts are present, a filter is applied to smooth the contrasts in the density and the compressibility functions to avoid numerical artifacts associated with Gibbs phenomenon. Causal attenuation is introduced through a generalized compressibility, determined by a series of relaxation mechanisms. The number of relaxation processes are adjusted until the resulting attenuation matches the measured dependence on frequency. However, as pointed out by Sushilov and Cobbold (2004), evidence is not currently available to support the view that multiple relaxation mechanisms are responsible for the intrinsic attenuation in media such as biological tissue in which the exponent differs from two (2). Methods such as the k-space method have the attractive feature of being less computer intensive, since it allows for large time and spatial steps than a FDTD method. On the other hand, solving the problem through direct solution of the wave equation via finite differences with due regard to attenuation and dispersion, without resorting to global manipulations or to filtering, can provide the most precise discrete, exact solution to the problem, when computationally affordable.

Additionally, fractional caculus has been used as an empirical method to describe the properties of viscoelastic materials. The observation that

asymptotic expressions of stiffness and damping in porous materials are proportional to the fractional powers of frequency suggests that time derivatives of a fractional order might describe the behavior of sound waves in this kind of material, including relaxation and frequency dependence [Fellah, Wirgin, Fellah, Sebaa, Depollier, and Larusiks (2005)].

Szabo (1994) proposed a way to include attenuation and dispersion effects directly in the time-domain through the inclusion of a causal convolutional propagation operator into the wave equation for media whose attenuation is described by a power law. Waters, Hughes, Brandenburger, and Miller (2000) showed that Szabo's operator could be used for a broader class of media, provided the attenuation possess a Fourier transform in a distributional sense Waters, Mosley, and Miller (2005). Norton and Novarini (2003) clarified the use of the operator and demonstrated its validity by solving the inhomogeneous wave equation including the causal convolutional propagation operator via a FDTD scheme. All computations were performed entirely in the time-domain. It was shown that the inclusion of the operator in modeling propagation in a homogeneous, weakly dispersive medium correctly carries the information on attenuation and dispersion into the time-domain. The method was first applied to a medium whose attenuation was described by a power law. And then to a medium possessing a bell-shaped attenuation profile, i.e., zero at zero frequency, peaks and decreases to zero as the frequency goes to infinity. This is the typical behaviour of most materials and solutions when an extended frequency band is considered (e.g., bubbly liquids, suspensions, seawater, etc). Next, as a measure of the effectiveness of using the local operators to model a spatially varying medium, the convolutional propagation operator was used to model 2-D pulse propagation in the presence of an interface separating two dispersive media [Norton and Novarini (2004)]. The attenuation used in both media was of the generic type described above. It was shown that the use of the operator leads to the correct reflected and transmitted fields. Additionally this technique has been used to describe scattering from and propagation through bubble clouds in the ocean [Norton and Novarini (2006)]. More recently, Sushilov and Cobbold (2004) derived an exact analytical time-domain solution for propagation in a homogeneous, dispersive medium obeying a power law function describing the attenuation for exponents between 0 and 3. Results were compared with the numerical solution obtained by Norton and Novarini (2003) for the case of the linear power law showing excellent agreement.

In this work the ability of the operator to bring attenuation and dispersion into the scattering problem of a localized scatterer, with impedance contrast typical of biological tissues is examined. To that end, 2D scattering from a fluid, lossy infinite cylinder with acoustic properties of biological tissue is modeled. Biological tissues are soft and do not support shear waves, therefore they can be treated as a lossy fluid. In this work, where the operator is based on causality, the origin of the losses include all mechanisms that remove energy from the beam within a given tissue (viscosity, thermal loss, and scattering by micro-inhomogeneities within the tissue). Causality, invoked through the Kramers-Kronig (K-K) relations leading to the operator, relates the total attenuation with its corresponding dispersion. The input information will be the frequency dependent attenuation, usually available in empirical form. The causal sound speed associated with it is automatically included through the convolutional propagation operator. The FDTD method adopted is 4th order in space and time, thus minimizing the intrinsic grid dispersion to negligible levels. It will also be shown that with adequate spatial and temporal sampling, high impedance contrast requires no special handling by the model. Numerical solutions are benchmarked against exact solutions synthesised from a frequency-domain solution (cw), which makes use of the effective attenuation and dispersion implicitly contained in the operator. A normal-mode solution for a fluid cylinder with density and sound speed contrast is adopted [Stanton (1988)] as the reference solution. Attenuation is included by making the wavenumber complex [Vogt, Flax, Dragonette,

and Neubauer (1975)].

In this work it is shown that the inclusion of the convolutional propagation operator into the linear wave equation, produces the correct scattered field for a variety of tissues each having a unique power law attenuation form. Thus, the inclusion of the convolutional propagation operator in large-scale time-domain 4-4 finite-difference modeling of propagation of anatomically realistic tissue cross sections could lead to further improvement in the fidelity of the modeling results. This will be particularly useful when the synthetic field is used as input for image reconstruction algorithms, where dispersion may introduce distortion of the propagating waveform, as well as additional fluctuations in the time of arrival.

## 2 The convolution propagation operator

A brief review of the convolution propagation operator is now given. For details see [Szabo (1994); Waters, Hughes, Brandenburger, and Miller (2000); Norton and Novarini (2003)]. Assuming that propagation occurs through an isotropic lossy linear medium, the propagation is governed by a modified wave equation of the form

$$\nabla^2 p(r,t) - \frac{1}{c_0^2}\frac{\partial^2 p(r,t)}{\partial t^2} - \frac{1}{c_0} L_\gamma(t) * p(r,t) = \delta(r-r_s)\, s(t) \quad (1)$$

Where $c_0$ is a reference sound speed (usually the thermodynamic sound speed in the medium assumed lossless), $s(t)$ is the source signature at location $r_s$, and $L_\gamma(t)$ is the causal convolutional propagation operator, which controls the attenuation and dispersion. It plays the role of a generalised dissipative term in the time-domain. In the framework of generalised functions, assuming the pressure field is a distribution, this operator is defined as $L_\gamma(t) \equiv \Gamma(t) * \delta^{(1)}(t)$.

The function $\Gamma(t)$ is the kernel of the operator, and represents a causal time-domain propagation factor that accounts for causal attenuation. That is, it also governs the dispersion in the system in order to insure causality. It is the parameter that needs to be calculated. Equation (1) can be rewritten in terms of the time-domain propagation factor as

$$\nabla^2 p(r,t) - \frac{1}{c_0^2}\frac{\partial^2 p(r,t)}{\partial t^2} - \frac{1}{c_0}\frac{\partial\left(\Gamma(t) * p(r,t)\right)}{\partial t} = \delta(r-r_s)\, s(t) \quad (2)$$

In the frequency-domain, propagation in a dispersive medium can be described through a complex propagation factor

$$k(\omega) = -\alpha(\omega) + i\beta(\omega) \quad (3)$$

Where $\alpha(\omega)$ is the frequency dependent attenuation and $\beta(\omega) = \frac{\omega}{c_0} + \beta'(\omega)$ is the real wavenumber, with $\beta'(\omega)$ its dispersive component given by

$$\beta'(\omega) = \omega\left[\frac{1}{c(\omega)} - \frac{1}{c_0}\right]. \quad (4)$$

The complex propagation factor can also be expressed as

$$k(\omega) = \gamma'(\omega) + i\frac{\omega}{c_0}. \quad (5)$$

And $\gamma'(\omega) = -\alpha(\omega) + i\beta'(\omega)$ represents the dispersive component of the complex propagation factor. Szabo defined the causal time-domain propagation factor as the inverse Fourier transform of $\gamma'(\omega)$.

$$\Gamma(\tau) = F^{-1}\left\{\gamma'(\omega)\right\} \quad (6)$$

where $\tau$ is retarded time $\tau = t - r/c_0$. Since in weakly dispersive media $\alpha(\omega)$ and $\beta'(\omega)$ are related by causality through the (K-K) relations (they are the Hilbert transform of each other) then,

$$\beta'(\omega) = -H\left\{-\alpha(\omega)\right\} \quad (7)$$

Finally Szabo arrived with

$$\Gamma(\tau) = -21_+(\tau)\, FT^{-1}\left\{\alpha(\omega)\right\} \quad (8)$$

where $1_+(\tau)$ represents the step function defined as

$$1_+ = \left\{ \begin{array}{ll} 0 & \tau < 0 \\ \frac{1}{2} & \tau = 0 \\ 1 & \tau > 0 \end{array} \right\}. \quad (9)$$

Note all that is required to generate the causal time-domain propagation factor is the attenuation associated with the media in terms of frequency. This attenuation could be determined from analytical means or from experiment. Once the causal time-domain propagation factor is determined, Eq. (2) can be solved with both the medium's attenuation and associated sound speed dispersion incorporated into the solution.

## 3 Numerical modeling

### 3.1 The reference solution

The time-domain solution used as a benchmark is calculated via Fourier synthesis of cw solutions. In the frequency domain, an exact solution for 2-D scattering from an infinite fluid, lossy cylinder is available. A cw normal model solution for a fluid cylinder with density and velocity contrast is adopted [Mortesen, Edmonds, Gorfu, Hill, Jensen, Schattner, Shifrin, Valdes, Jeffrey, and Esserman (1996)] assuming a cylindrical incident wave generated by a line source, instead of a plane wave. Attenuation is included by making the wavenumber complex [Stanton (1988)]. Given a frequency dependent attenuation, the associated sound speed dispersion is calculated via causality through the K-K relations, implicitly invoked and obtained as a by-product in the generation of the causal time-domain propagation factor [Eq. (8)]. The following are the boundary conditions on the cylinder, the pressures are equal on each side of the interface as are the normal components of the particle velocity equal on each side of the interface.

The scattered pressure is given by

$$p_{scat}(t,r) = e^{-i\omega t} P_{inc} \sum_{m=0}^{\infty} b_m i^m H_m^{(1)}(kr) \cos m\phi \quad (10)$$

with $r$ the distance from the source to the center of the cylinder, $\phi$ the azimuthal angle between the incident and scattered wave (0deg is backscattering), $k$ the incident wave number, and the function $b$ is given by,

$$b_m = \frac{-\varepsilon_m}{1 + iC_m} \quad (11)$$

where $\varepsilon_m$ is the Neumann factor ($\varepsilon_m = 1$ for $m = 0$ and 2 for $m = 1, 2, ..$) and the function $C$ is given by

$$C_m = \frac{J'_m(k_1 a) N_m(ka) - ghN'_m(ka) J_m(k_1 a)}{J'_m(k_1 a) J_m(ka) - ghJ'_m(ka) J_m(k_1 a)} \quad (12)$$

where $J_m(x)$ and $N_m(x)$ are the cylindrical Bessel and Neumann functions and the primes denote their derivatives, and the functions $g$ and $h$ are the ratios of the densities ($g = \rho_1/\rho_0$) and sound speed ($h = c_1/c_0$).

In the case of a line source the incident field on the cylinder (the field at the location of center of the cylinder in the absence of the cylinder) is given by

$$P_{inc} = A(f) H_0^1(k(\omega) r) \quad (13)$$

with $A(f)$ the spectral amplitude of the source function. Note that for dispersive media, the arguments of the cylindrical functions become complex. In this work the sound speed inside the cylinder is a function of frequency. To accommodate attenuation, the wavenumber in the interior of the cylinder is complex, $k_1 = [2\pi f/c_1(f)][1 + i\delta(f)]$, where $\delta(f) = c_1(f)\alpha(f)/2\pi f$, and $\alpha$, the attenuation in $Neper/m$. In this case the argument of the Bessel and Neumann functions are complex. The series in Eq. (10) converges quite quickly. For all numerical calculations fifty terms were used.

### 3.2 Finite-difference-time-domain scheme

The solution of Eq. (2) originally was expressed in terms of finite-differences using the classical explicit second-order scheme in time and fourth-order in space. However, to make the algorithm uniformly fourth-order accurate, the second partial of the field with respect to time had to be extended to fourth-order. The usual fourth-order

finite-difference representation of the second partial derivative would lead to unconditionally unstable schemes. A technique presented by Cohen (2001), based on the "modified equation approach", was used to obtain fourth-order accuracy in time. This technique while improving the accuracy in time preserves the simplicity of the second-order accurate time-step scheme. Absorbing Boundary Conditions (ABCs) were imposed at the end of the numerical grid and at the corners. A technique named the Complementary Operators Method (COM) was employed [Schneider and Ramahi (1998)]. The COM is a differential equation-based ABC. This differs from the other common approach of terminating the grid with the use of an absorbing material. An example of this type of boundary condition is the Perfectly Matched Layer (PML) method originally proposed by Berenger (1994). Implementation of the ABCs via the COM requires only two grid points around the perimeter of the computational domain.

It is beyond the scope of this paper to present the derivation of either the fourth-order accurate time derivative algorithm or the implementation of the COM operators. The interested reader should refer to Norton and Novarini (2005). The resulting computer model is designated causal-FDTD.

### 3.3 Numerical experiments

An infinite circular cylinder 7mm in radius is ensonified by a line source parallel to its axis. The cylinder has the acoustic properties of a biological tissue. Five tissues are examined; brain, liver, kidney, heart and tendon. The attenuation for each tissue is described by a power law whose functional form is of the type $\alpha(\mathrm{f}) = \mathrm{bf}^{\mathrm{y}}$. Units are in $dB/cm$ with $b$ in units of $dB/cm/MHz^y$. The parameters are taken from Edmonds and Dunn (1981) and Gross, Johnston, and Dunn (1978), and are listed in Table I. For simplicity, the surrounding (background) medium is water ($\rho_0 = 1gr./cc, c_0 = 1500m/s$) and thus, the assumption is that dispersion can be neglected in this medium (the case of two dispersive media in contact was already addressed in Norton and Novarini (2004)). The modeling is carried out in 2-D. Backscattering in the direction of the source ($\phi = 0$) is modeled. The source is located $140mm$ from the center of the cylinder, with its axis parallel to the cylinder. The receiver is located between the cylinder and the source, co-linear with the source-receiver direction, at $14mm$ from the center of the cylinder.

The cylinder is interrogated by a broadband signal, with a source function (a doublet in this case) of the form

$$s(t) = te^{-\mu t^2} \tag{14}$$

where $\mu$ is a constant governing the time interval between the negative and positive peaks of the doublet. Its amplitude spectrum is given by

$$A(\omega) = \frac{\pi^{1/2}\omega}{2\mu^{3/2}} \exp\left(-\frac{\omega^2}{4\mu}\right) \tag{15}$$

The peak frequency (in $Hz$) is given by

$$f_{pk} = \frac{\sqrt{2\mu}}{2\pi}. \tag{16}$$

For the desired peak frequency ($500kHz$) the constant $\mu$ is chosen equal to $4.93 \times 10^{12}$.

In the current implementation of Szabo's approach, when attenuation increases monotonically with frequency (as it is for the case when the attenuation is described by a power law function) it is necessary to generate the attenuation function over a much wider frequency range than the source bandwidth. A window function is then applied that leaves invariant the region of interest (e.g., source bandwidth defined at half-power). This is done to avoid introducing artifacts stemming from the numerical implementation of Eq. (8) to generate the time-domain propagation factor $\Gamma(t)$. In this case, a Hamming window centered at zero $Hz$ was applied over the entire frequency range. The frequency increment ($\delta f$) is $5714.5Hz$ and the number of frequencies is equal to 4096. This methodology has been successfully verified in a previous work [Norton and Novarini (2003)]. It was demonstrated that upon propagation between two points using the FDTD solution in an isotropic medium, the retrieved attenuation and dispersion are in agreement with the theoretical expectations over the bandwidth of interest.

As explained elsewhere, the frequency dependence of the attenuation is the required information from which the time-domain propagation factor and hence the convolutional propagation operator, is generated. Detailed information pertaining to the physical properties of mammalian tissues in the literature is scarce. Even scarcer is information on the spectral description of the attenuation. In most cases partial information is provided, e.g. attenuation at a specific frequency, implicitly assuming a linear dependence with frequency. In this work the spectral description of the attenuation at $37C$ for five tissues as given by Gross, Johnston, and Dunn (1978) and summarized in Edmonds and Dunn (1981) is adopted (Table I), where the coefficients $b$ and $y$ defining the functional form were found by regression fittings. To obtain the corresponding sound speed at each frequency, necessary to obtain the cw solution from which the expected results are synthesized, a unique reference sound speed $c_0$ is required for each tissue. These values are not readily available. However, for each of the selected tissues, sound speed has been reported at specific frequencies. The procedure adopted in this work was to generate the Hilbert transform of the known attenuation, which returns the dispersive part $\beta'$ of the total wavenumber (Eq. (7)) in order to form the sound speed assuming different values of the reference speed $c_0$. This procedure was continued until finding the $c_0$ that when combined with $\beta'$, as prescribed in Eq. (4), produces the reported value of $c(w)$ at the particular frequency. The density is uniformly set to $1.0gr./cc$. Table I lists the spectral parameters ($b$ and $y$) describing the attenuation function, along with the adopted reference speed and the reported density.

The causal-FDTD modeling was accomplished using the following parameters. The spatial step in both the $X(\delta X)$ and $Z(\delta Z)$ direction was equal to $7.0\times10^{-5}m$. The number of grid points in the $X$ direction equaled 5000 and the number of grid points in the $Z$ direction was 2500. The time step used was $\delta t = 2.13623\times10^{-8}$ sec. The computer model is parallelized over 40 processors, running on a CRAY MTA 2. The geometry is shown in Fig. 1. The number of grid points inside the cylinder that required solving Eq. (2) was 31599. The maximum number of convolution terms at each of these grid points was 1024. Each run took approximately 45 minutes of wall clock time.

Table 1: Parameters describing the modeled tissues

| Tissue | $b[dB/cm/MHz^y]$ | $y$ | $C_0[m/s]$ |
|---|---|---|---|
| Brain | 0.607 | 1.14 | 1541 |
| Heart | 1.128 | 1.07 | 1586 |
| Kidney | 0.868 | 1.09 | 1563 |
| Liver | 0.690 | 1.13 | 1580 |
| Tendon | 4.860 | 0.763 | 1780 |

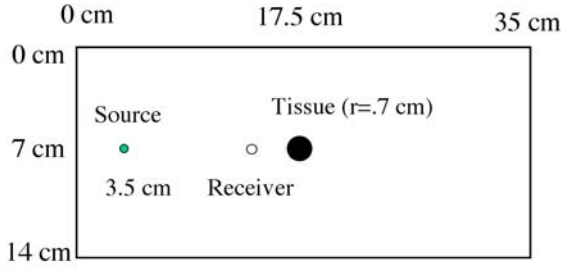


Figure 1: Geometry of numerical expriment

## 4 Results

Figures 2 and 3 depict the attenuation and phase speed for the tissues over a frequency band larger than the source bandwidth. The source bandwidth is $2.5MHz$. Within this interval, the window imposed on the original attenuation function to generate the propagation factor has negligible effect, thus retaining the original functional form. Note that the attenuation and phase speed for the tendon is markedly different compared to the other tissues. Figure 4 displays the causal time-domain propagation factor, calculated from Eq. (8), for the five tissues. Only the earlier times are shown. For later times, in all cases the functional form decays monotonically to zero. Notice that the time-domain propagation factor for the

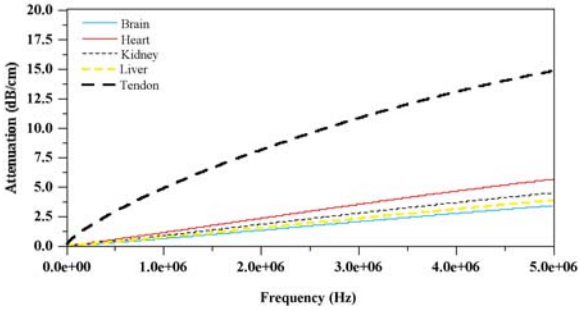


Figure 2: Attenuation vs. tissue type

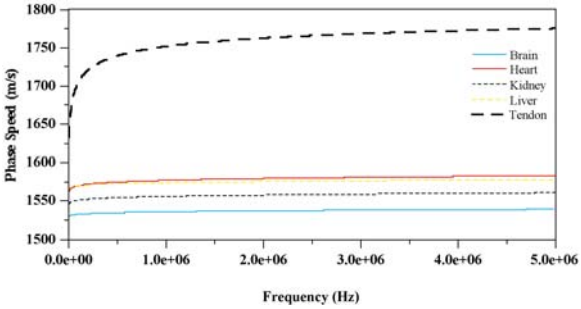


Figure 3: Phase speed vs. tissue type

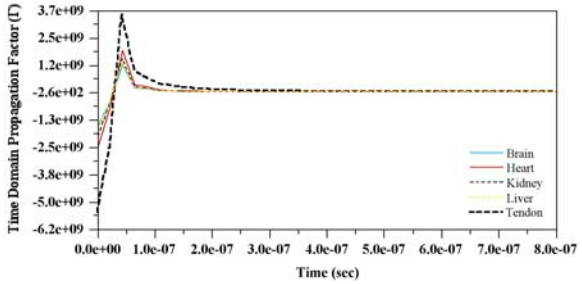


Figure 4: Time-domain propagation factor vs. tissue type

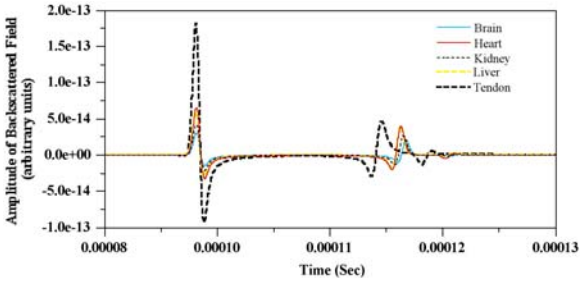


Figure 5: Synthesized backscatter amplitude vs. tissue type

tendon is markedly different/stronger than those for the other tissues, which follows the difference observed with the attenuation and phase speed of Fig. 2 and 3. Figure 5 shows the backscatter response of the tissue synthesized from the CW approach for the different tissues. The density for each tissue was set equal to $1.0 gr./cc$, so as to compare with results from the current version of the causal-FDTD model. As expected the tendon shows the largest initial reflection due to its large impedance contrast. The reference sound speed is $1780 m/s$. And as a consequence the second arrival occurs sooner than for the other tissues. This second arrival results from the sound penetrating the tissue, traveling to the back wall and reflecting back and exiting the tissue and traveling to the receiver. The third arrival which is most pronounced with the tendon, results from a circumferentially traveling wave.

Figure 6 shows the comparison of results obtained via the causal-FDTD model versus the expected values synthesized from the exact CW solution shown in Fig. 5 for the simulated brain tissue. The comparison between the causal-FDTD result and those synthesized from the exact CW solution for the simulated heart, kidney and liver are nearly identical to those for the simulated brain tissue and hence are not shown. Figure 7 compares the causal-FDTD result and those synthesized from the exact CW solution for the simulated tendon tissue. The tendon result is shown since it represents a more demanding case. Due to its dispersive characteristics being markedly stronger than the other tissues (See Figs. 2 and 3.) its backscatter response is likewise markedly different than the other four simulated tissues. In all cases the results are normalized to the peak value of the reflected return. Generally, the causal-FDTD matches the exact results with high accuracy. There are noticeable differences that occur between the first and second arrival for all tissues. The causal-FDTD solution has a noticeable interference or modulation of the signal between these two arrivals. Other than this discrep-

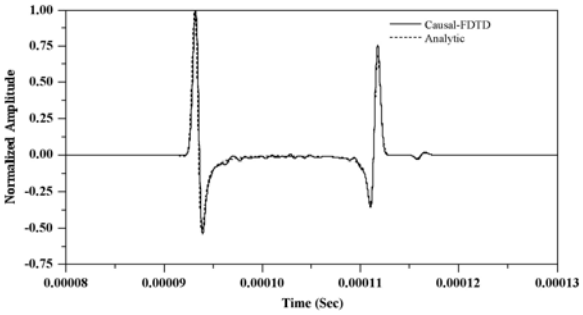


Figure 6: Comparison of the normalized backscatter field for simulated brain tissue

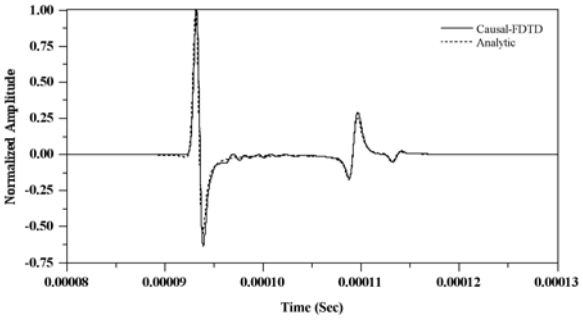


Figure 7: Comparison of the normalized backscatter field for simulated tendon tissue

ancy the arrival structure matches the analytic solution in both relative amplitude and time to a high degree. This demonstrates that the use of the local convolutional propagation operator (introduced through the time-domain propagation factor) brings the correct impedance contrast (produced by the change in sound speed and attenuation) into the model within the pulse bandwidth. It also demonstrates that the FDTD model as implemented (4th order in space and 4th order in time), correctly handles the impedance contrast in the scattering process with no noticeable grid dispersion.

To illustrate the importance of including dispersion (and causal attenuation) in the scattering problem, Fig. 8 compares the results for the tendon assuming first that it is non-dispersive ($\alpha = 0$ and $c_2 = c_0 = 1780m/s$ for all frequencies) (solid line) and then dispersive (i.e., $\alpha(f)$ and $c_2(f)$) (dotted line). As expected the major difference

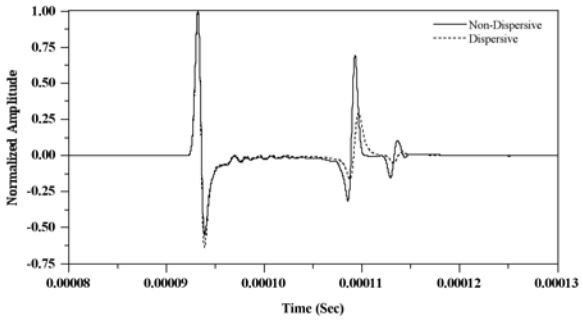


Figure 8: Comparison of the normalized backscatter field for simulated non-dispersive tendon tissue (solid line) with dispersive tendon tissue (dotted line).

occurs for the second and third returns. The second return which is due to the signal traveling through the tissue, hitting the other side and returning, arrives at the receiver at an earlier time and with a higher amplitude than that resulting from a dispersive tissue. This is because the all frequencies experience the same sound speed inside the tissue namely $c_0 = 1780m/s$, which is faster than the phase speed in the dispersive case. In addition there is no attenuation, thus the amplitude is much large for the dispersive case. Additionally the temporal width of the positive portion of this return is very similar to the return due to the reflection. Note the signal is not spreading in time, as is the signal in the dispersive tissue. Finally note that the third return, resulting from the circumferentially traveling wave, for the non-dispersive case is much stronger than for the dispersive case and further the signal arrives at the receiver sooner than for the dispersive case. It is apparent that the presence of dispersion dramatically alters the backscattered signal in both amplitude and temporal location.

## 5 Concluding remarks

Direct time domain modeling of transient 2D scattering by a localized object, with dispersive acoustic properties representative of biological tissues, has been performed via direct numerical solution of the modified linear wave equation for an inhomogeneous medium, which in-

cludes attenuation and dispersion while remaining entirely in the time-domain (causal-FDTD). It was demonstrated that the inclusion of Szabo's causal convolutional operator acting as the only descriptor of the object, successfully reproduces the scattered field for a variety of tissues, each one described by a different power law. This finding adds to previous findings, where it was shown that the use of the local operator to delimit regions of different dispersive properties accurately reproduces the reference solution. The method provides an exact solution for propagation and scattering in inhomogeneous dispersive media, and has the attractive attribute that it only requires the functional form of the attenuation (empirical or analytic) within the bandwidth of the signal for the tissues involved. Although computationally more intensive than approximate methods, the causal-FDTD method has the attractiveness of producing the most direct, exact solution to the problem. It can be used for high fidelity time-domain modeling of sound propagation through and scattering from complex anatomical structures, including high contrast scatteres, with highly accurate amplitude and timing of the transient arrivals and wavefront distortion.

**Acknowledgement:** This work has been supported by the Office of Naval Research (Program element No. 61153N) and by a grant of computer time at the DoD High Performance Computing Shared Resource Center (Naval Research Laboratory, Washington, D. C.). This document has been reviewed and is approved for public release.

## References

1. **Berenger, J. P.** (1994): A perfectly matched layer for the absorption of electromagnetic waves. *J. Comp. Phys.*, vol. 114, pp. 185–200.

2. **Cohen, G.** (2001): *Higher-Order Numerical Methods for Transient Wave Equations* . Springer-Verlag, Berlin.

3. **Edmonds, P. D.; Dunn, F.** (1981): *Introduction: Physical description of ultrasonic fields, in: Methods of Experimental Physics: Ultrasonics*. Academic Press, New York.

4. **Fellah, Z. E.; Wirgin, A.; Fellah, M.; Sebaa, N.; Depollier, C.; Larusiks, W.** (2005): A time-domain model of transient acoustic wave propagation in double-porous media. *J. Acoust. Soc. Am.*, vol. 118, pp. 661–670.

5. **Gross, S. A.; Johnston, R. L.; Dunn, F.** (1978): Comprehensive compilation of empirical ultrasonic properties of mammalian tissues. *J. Acoust. Soc. Am.*, vol. 64, pp. 423–457.

6. **Lizzi, F. L.; Greenebaum, M.; Feleppa, E. J.; Elbaun, M.; Coleman, D. J.** (1983): Theoretical framework for spectrum analysis in ultrasonic tissue characterization. *J. Acoust. Soc. Am.*, vol. 73, pp. 1366–1373.

7. **Manry, C. W.; Broschat, S. L.** (1996): FDTD Simulations for Ultrasound Propagation I a 2-D breast model. *Ultrasonics Imaging*, vol. 18, pp. 25–34.

8. **Mast, T. D.; Hinkelman, L. M.; Orr, M. J.; Sparrow, V. W.; Waag, R. C.** (1997): Simulation of ultrasonic pulse propagation through the abdominal wall. *J. Acoust. Soc. Am.*, vol. 102, pp. 1177–1190.

9. **Mast, T. D.; Hinkelman, L. M.; Orr, M. J.; Sparrow, V. W.; Waag, R. C.** (1998): The effect of the abdominal wall morphology on ultrasonic pulse propagation. Part II. Simulations. *J. Acoust. Soc. Am.*, vol. 104, pp. 3651–3664.

10. **Mortesen, C. L.; Edmonds, P. D.; Gorfu, Y.; Hill, J. R.; Jensen, J. F.; Schattner, P.; Shifrin, L. A.; Valdes, A. D.; Jeffrey, S. S.; Esserman, L. J.** (1996): Ultrasound tissue characterisation of breast biopsy specimens: expanded study. *Ultrasonic Imaging*, vol. 18, pp. 215–230.

11. **Norton, G. V.; Novarini, J. C.** (2003): Including dispersion and attenuation directly in the time domain for wave propagation in

isotropic media. *J. Acoust. Soc. Am.*, vol. 113, pp. 3024–3031.

12. **Norton, G. V.; Novarini, J. C.** (2004): Including dispersion and attenuation in time domain modeling of pulse propagation in spatially-varying media. *J. Comp. Acoust.*, vol. 113, pp. 1–19.

13. **Norton, G. V.; Novarini, J. C.** (2005): Time domain modeling of pulse propagation in non-isotropic dispersive media. *Math. Comp. Sim.*, vol. 69, pp. 467–476.

14. **Norton, G. V.; Novarini, J. C.** (2006): Finite-differencve time-domain simulation of acoustic propagation in dispersive medium: An application to bubble clouds in the ocean. *Comp. Phys. Comm.*, vol. 174, pp. 961–965.

15. **Schneider, J. B.; Ramahi, O. M.** (1998): The complementary operators method applied to acoustic finite-difference time-domain simulations. *J. Acoust. Soc. Am.*, vol. 104, pp. 686–693.

16. **Stanton, T. K.** (1988): The complementary operators method applied to acoustic finite-difference time-domain simulations. *J. Acoust. Soc. Am.*, vol. 83, pp. 55–63.

17. **Sushilov, N. V.; Cobbold, R. C.** (2004): Frequency-domain wave attenuation and its time-domain solutions in attenuating media. *J. Acoust. Soc. Am.*, vol. 115, pp. 1431–1436.

18. **Szabo, T. L.** (1994): Time domain wave equations for lossy media obeying a frequency power law. *J. Acoust. Soc. Am.*, vol. 96, pp. 491–500.

19. **Tabei, M.; Mast, T. D.; Waag, R. C.** (2002): A k-space method for coupled first order acoustic propagation equations. *J. Acoust. Soc. Am.*, vol. 111, pp. 53–64.

20. **Tabei, M.; Mast, T. D.; Waag, R. C.** (2003): Simulation of ultrasonic focus aberration and correction through human tissue. *J. Acoust. Soc. Am.*, vol. 113, pp. 1166–1176.

21. **Vogt, R. H.; Flax, L.; Dragonette, L. R.; Neubauer, W. G.** (1975): Monostatic reflection of a plane wave from an absorbing sphere. *J. Acoust. Soc. Am.*, vol. 57, pp. 558–561.

22. **Waters, K. R.; Hughes, M. S.; Brandenburger, G. H.; Miller, J. G.** (2000): On a time-domain representation of the Kramers-Kronig dispersion relations. *J. Acoust. Soc. Am.*, vol. 108, pp. 2114–2119.

23. **Waters, K. R.; Mosley, J.; Miller, J. C.** (2005): Causality-imposed (Kramers-Kronig) relationships between attenuation and dispersion. *IEEE Trans. Ultrasonics*, vol. 52, pp. 822–833.